SCHEDULING OF MULTISTATIC SONOBUOY FIELDS USING MULTI-OBJECTIVE OPTIMIZATION

C. Gilliam[1], *D. Angley*[2], *S. Suvorova*[2], *B. Ristic*[1], *B. Moran*[2], *F. Fletcher*[3], *H. Gaetjens*[3] *and S. Simakov*[3]

[1] School of Engineering, RMIT University, Australia
[2] Electrical & Electronic Engineering, The University of Melbourne, Australia
[3] Maritime Division, Defence Science Technology Group, Australia

ABSTRACT

Sonobuoy fields, comprising a network of transmitters and receivers, are commonly deployed to find and track underwater targets. For a given environment and sonobuoy field layout, the performance of such a field depends on the scheduling, that is, deciding which source should transmit, and which from a library of available waveforms should be transmitted at any given time. In this paper, we propose a novel scheduling framework based on multi-objective optimization. Specifically, we pose the two tasks of the sonobuoy field—tracking and searching—as separate, competing, objective functions. Using this framework, we propose a characterization of scheduling based on Pareto optimality. This characterization describes the trade-off between the search-track objectives and is demonstrated on realistic multistatic sonobuoy simulations.

***Index Terms*—** Multi-static sonar; Sensor scheduling; Multi-objective optimization; Target tracking; Pareto optimality

1. INTRODUCTION

A multistatic sonobuoy field comprises a network of transmitters (sources) and receivers distributed across a large search area, used to search for and track underwater targets. The network operates by emitting an acoustic signal, or "ping", from a transmitter sonobuoy and receiving the signal, possibly reflected from a target, at nearby receivers. In our context, the ping is either a frequency modulated (FM) signal to measure target range and bearing, or a continuous wave (CW) signal, to detect moving targets and to provide target bearing and Doppler information as well as coarse range measurements. By fusing the measurements, this network of sensors is able to achieve high target detection performance in challenging underwater environments where the signal-to-noise ratio of the returned signal is typically low and clutter is significant. An example of a sonobuoy field with 16 sources and 25 receivers is shown in Fig. 1. The blue and green lines represent trajectories of targets that the field must find and track. For this work, a key aspect, however, is to decide which transmitter should ping in order to optimize the performance of these search and track tasks.

The sequential order in which the sources in the network transmit, and which waveform they use, is governed by a central scheduler (i.e. sensor manager). Krout et al [1] were the first to identify that the performance of a multistatic sonobuoy system could be improved via intelligent scheduling. They developed a framework for *greedy* (or myopic) scheduling with separate metrics for search and tracking. Since then significant work has been undertaken to define new metrics and greedy algorithms for scheduling. For example, search metrics based on the probability of undetected targets in the field have been investigated using diffusion concepts in [1, 2], Monto-Carlo techniques in [3, 4], and extended to incorporate target track information in [5]. In contrast, metrics based on weighting the track information were proposed in [6], and optimizing the expected number of target detections in [7]. *Long term* (non-myopic) scheduling has been investigated in [8–11].

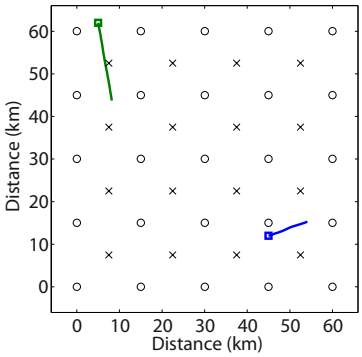

Fig. 1. Illustration of a multistatic sonobuoy field and targets. The crosses are transmitter sonobuoys and the circles are receivers. The coloured lines indicate target trajectories and the squares indicate their starting point.

In this paper, we propose a novel myopic multi-objective framework for scheduling. Specifically, we treat the search and track tasks as competing objectives and use multi-objective optimization to decide the source and waveform at a given transmission time. In contrast to single-objective optimization, multi-objective problems in general have no single solution as their objectives may conflict with one another [12]. For example, tracking could involve transmitting in a area of the field that has already been searched. Thus, different solutions are obtained depending on how the objectives are prioritized. We formulate this prioritization using the weighted sum method [13] — the objectives are combined as a convex sum, and different solutions are obtained for different weightings. To assess these solutions, we use *Pareto optimality* [14]: a point is Pareto optimal if there is no other point that improves at least one objective function without detriment to another objective. Accordingly, we present a characterization of scheduling in terms of a set of Pareto optimal points, known as the *Pareto front*, that describe the trade-off in the search-track objectives. This characterization is demonstrated using realistic multistatic sonobuoy simulations. Note that, in terms of tracking, multi-objective techniques have previously been proposed for waveform design in radar [15] and sensor selection in

This research was supported in part by Defence Science and Technology under the Research Agreement "Sensor Scheduling for Multistatic Sonar Systems".

wireless networks [16].

The paper is organised as follows. In Section 2, we review tracking in multistatic sonobuoy fields. In Section 3, we present the framework of our scheduling algorithm, in particular integration of the search and track tasks into a multi-objective problem. We then analyse our scheduler using simulations in Section 4, followed by a concluding section.

2. MULTISTATIC SONAR TRACKING

The key elements required to track a target in the sonobuoy field are introduced here.

2.1. Modelling and Measurements

As illustrated in Fig. 1, the multistatic sonobuoy field comprises a network of N_s sources and N_r receivers. The position of the jth source in the field is defined as $\mathbf{s}_j = \left[x_s^j, y_s^j\right]^{\mathrm{T}}$, where $j = 1, \ldots, N_s$ and the position of the ith receiver is defined as $\mathbf{r}_i = \left[x_r^i, y_r^i\right]^{\mathrm{T}}$, where $i = 1, \ldots, N_r$. We assume that the buoy positions are known at all times, and ignore any ocean drift effects in this paper. An underwater target within the field is described using the following time-varying state: $\mathbf{x}_k = [\mathbf{p}_k^{\mathrm{T}}, \mathbf{v}_k^{\mathrm{T}}]^{\mathrm{T}}$, where $\mathbf{p} = [x_k, y_k]^{\mathrm{T}}$ is the position of the target at time t_k and $\mathbf{v} = [\dot{x}_k, \dot{y}_k]^{\mathrm{T}}$ is its corresponding velocity. The motion of a target is approximated using the linear constant velocity model:

$$\mathbf{x}_k = f(\mathbf{x}_{k-1}) = \left(\begin{bmatrix} 1 & T \\ 0 & 1 \end{bmatrix} \otimes \mathbf{I}_2 \right) \mathbf{x}_{k-1} \tag{1}$$

where $T = t_k - t_{k-1}$ is the sampling in time, $\otimes$ is the Kronecker product and $\mathbf{I}_2$ is the 2×2 identity matrix. Note that, for this paper, we assume that the targets remain at a constant depth.

Given the above geometric model, when a source emits a ping, we obtain a set of measurements $\mathbf{Y}_k^{(i)}$ collected by a subset of receivers $i \in I_k$, known as the proximal (or contributing) receivers. These measurements may relate to an actual target within the field or a phantom target created by a false detection. Individually, a measurement $\mathbf{y} \in \mathbf{Y}_k^{(i)}$ comprises the kinematic measurement $\mathbf{z}$ and the returned signal amplitude β such that $\mathbf{y} = [\beta, \mathbf{z}^{\mathrm{T}}]^{\mathrm{T}}$. The components of the kinematic measurement $\mathbf{z}$ depend upon the type of waveform emitted by the source. If an FM waveform has been emitted, then $\mathbf{z}$ contains the bistatic range — the range from the source to the target to the receiver — and the angle from the receiver. Whereas, if a CW waveform is used, then, in addition to the bistatic range and the angle from the receiver, the vector $\mathbf{z}$ also includes the bistatic range-rate. Accordingly, for a waveform ϕ, we have:

$$\mathbf{z} = \mathbf{h}_{j,\phi}^{(i)}(\mathbf{x}_k) + \mathbf{w}_{j,\phi}^{(i)} \tag{2}$$

where $\mathbf{h}_{j,\mathrm{FM}}^{(i)}(\mathbf{x}_k) = \left[h_{j,\rho}^{(i)}(\mathbf{x}_k), h_{j,\theta}^{(i)}(\mathbf{x}_k)\right]^{\mathrm{T}}$ when $\phi = \text{FM}$ and $\mathbf{h}_{j,\mathrm{CW}}^{(i)}(\mathbf{x}_k) = \left[h_{j,\rho}^{(i)}(\mathbf{x}_k), h_{j,\theta}^{(i)}(\mathbf{x}_k), h_{j,d}^{(i)}(\mathbf{x}_k)\right]^{\mathrm{T}}$ when $\phi = \text{CW}$. The individual components are defined as

$$h_{j,\rho}^{(i)}(\mathbf{x}_k) = |\mathbf{p}_k - \mathbf{r}_i| + |\mathbf{p}_k - \mathbf{s}_j|\,, \;\; h_{j,\theta}^{(i)}(\mathbf{x}_k) = \tan^{-1}\!\left(\frac{y_k - y_r^i}{x_k - x_r^i}\right)$$

$$h_{j,d}^{(i)}(\mathbf{x}_k) = -\mathbf{v}^{\mathrm{T}} \left[\frac{\mathbf{p}_k - \mathbf{r}_i}{|\mathbf{p}_k - \mathbf{r}_i|} + \frac{\mathbf{p}_k - \mathbf{s}_i}{|\mathbf{p}_k - \mathbf{s}_i|} \right].$$

Lastly, $\mathbf{w}_{j,\phi}^{(i)}$ is zero-mean Gaussian noise with covariance $\mathbf{R}_{j,\phi}^{(i)}$.

2.2. Measurement Simulation Environment

To generate realistic multistatic sonobuoy measurements, we use BRISE — the Bistatic Range Independent Signal Excess simulation environment described in [17]. In brief, the environment works as follows: the target detection process is based on calculating a realization of the signal-to-noise-ratio (SNR) for each target at each receiver. This SNR calculation employs precomputed signal excess component data, stored in look-up tables, that depend on the configuration of the sources and receivers, the waveform emitted and the target depth. Computation of the signal excess component data is carried out offline using the Gaussian ray bundle eigenray propagation model [18]. Using this SNR value, BRISE then decides whether a detection has occurred and, if so, it provides the measurement vector $\mathbf{z}$ corrupted by additive Gaussian measurement noise (the covariance $\mathbf{R}_{j,\phi}^{(i)}$ of the noise is set in BRISE). False alarms are also generated using a Poisson distribution to determine the number of false detections and a uniform distribution from which to draw the elements of the measurement vector $\mathbf{z}$. For a complete review of the BRISE simulation environment see [7, 19].

2.3. Tracking Algorithm

Many algorithms have been proposed for tracking multiple underwater targets using a multistatic sonar field, for example see [20, 21]. In this paper, however, we opt for the robust multi-target multi-sensor Bernoulli tracker recently proposed in [19]. The tracker combines the optimal Bayesian multi-sensor filter for a single target in clutter, also known as the multi-sensor Bernoulli filter [22–24], with the linear-multi-target paradigm [25]. This choice is based on two key features of the tracker: 1) exploitation of the signal amplitude measurement associated with a detected target yields robust track initiation and false track discrimination; 2) capability to process measurements with different modalities (i.e. measurements from CW and FM waveforms). Note that we use the Gaussian mixture model implementation of this tracker outlined in [26].

3. MULTI-OBJECTIVE SCHEDULING FRAMEWORK

We now detail our multi-objective framework for scheduling the transmitters in the sonobuoy field. At each transmission time, the scheduler must choose one action a from the following action space

$$\mathcal{A} = \mathcal{S} \times \mathcal{W} \tag{3}$$

where $\mathcal{S} = \{j_1, \ldots, j_{N_s}\}$ is the set of all sources, $\mathcal{W} = \{w_1, \ldots, w_{N_w}\}$ is the set of all waveforms and $\times$ represents the Cartesian product of the two sets. In terms of waveforms, each transmitter has $N_w = 8$ options: it can choose to emit either a FM or CW waveform, at a frequency of either 1 kHz or 2 kHz frequency and with a transmission duration of either 2 seconds or 8 seconds.

For each of these actions, we assign two rewards: i) a reward, R_{search}, for searching the sonobuoy field to detect unknown targets and ii) a reward, R_{track}, for continued, high-quality, tracking of known targets. In this paper, we use the weighted sum method [27] to combine the tracking and search objectives. Accordingly, the scheduler picks a sequence of actions that maximises the following convex sum at each transmission time

$$\max_a \; \alpha R_{\text{track}}(a) + (1 - \alpha) R_{\text{search}}(a), \tag{4}$$

where $\alpha \in [0, 1]$ is the parameter that controls the priority the scheduler puts on searching versus tracking. The scheduler's overall performance in each task is thus dependent on the choice of α. We use

Pareto optimality to characterize how the performance in each task varies with α. In the following we outline the two reward functions.

3.1. Tracking Rewards

Given the prior tracking information, our reward function should measure the improvement in this information obtained from an action a. A suitable approach, commonly used in sensor management problems [28–30], is to approximate the Fisher information of the future tracker states relating to the location variables. Accordingly, our tracking reward takes into account the estimation accuracy as well as the probability of detection for the current tracks as follows: for an action $a \in \mathcal{A}$, assuming L current, confirmed, tracks, the tracking reward is:

$$R_{\text{track}}(a) = \sum_{\tau=1}^{L} \omega_k^\tau \text{ tr} \left[\mathbf{J}_p^\tau + \sum_{i \in I_k(a)} P_d^{\tau,i}(a)\, \mathbf{J}_m^{\tau,i}(a) \right] \quad (5)$$

where tr represents the trace of a matrix.

The first term in (5) corresponds to the prior (or predicted) Fisher information matrix for the track τ and is expressed as [31, Ch.4]

$$\mathbf{J}_p^\tau = \left[\mathbf{F}_{k-1}^\tau \mathbf{P}_{k-1}^\tau \left[\mathbf{F}_{k-1}^\tau \right]^{\text{T}} \right]^{-1}$$

where $\mathbf{F}_{k-1}^\tau$ is the Jacobian of the function $f(\mathbf{x})$, evaluated at $\mathbf{x}_{k-1}^\tau$, and $\mathbf{P}_{k-1}^\tau$ is the error covariance from the tracker. Assuming the motion model in (1), $\mathbf{F}_{k-1}^\tau$ is fixed and identical for all tracks. Note that we currently use only the position elements of the state vector when constructing the Fisher information. The second term in (5) corresponds to the information in the measurements obtained from the set of proximal receivers $I_k(a)$. This set is defined as the group of receivers that are within a circle centred at the source and with a radius twice that of the receiver-source separation. Individually, for a receiver i, the measurement contribution to the information matrix is [31, Ch.4]

$$\mathbf{J}_m^{\tau,i}(a) = \left[\mathbf{H}_k^{\tau,i}(a) \right]^{\text{T}} \left[\mathbf{R}_k^{\tau,i}(a) \right]^{-1} \mathbf{H}_k^{\tau,i}(a)$$

where $\mathbf{H}_k^{\tau,i}(a)$ is the Jacobian of the function $h_k^{\tau,i,a}$ defined in (2). This contribution is then weighted by $P_d^{\tau,i}(a)$, the expected probability of detection of track τ at receiver i given an action a. Finally, we use ω_k^τ to weight the information associated with each track. This weight is inversely proportional to the existence probability, given by the tracker defined in Section 2.3, and is normalised such that $\sum_\tau \omega_k^\tau = 1$. We only use confirmed tracks from the tracker, not tentative ones, when computing the reward function in (5).

3.2. Search Rewards

We calculate the search reward based on the change in the probability of undetected targets existing within the sonobuoy field when an action a is taken. Following [2], the presence of undetected targets are modelled using a drift/diffusion process on a discrete grid. The discrete grid, known as a threat map, spans the search region covered by the field and describes the probability of an undetected target existing within a cell of the grid. These probabilities evolve over time; they increase as undetected targets drift or diffuse into the search region and decrease when a nearby transmitter emits a ping.

The assumed drift and diffusion target motion process is implemented by filtering the threat map with a 2D filter G that describes the probability of a target entering from adjacent cells. In [2], this filter is obtained analytically by solving the Fokker-Planck equation. However, in order to accommodate target motion models that cannot be solved analytically, we use Monte-Carlo simulations to determine a more general filter. This method works by generating a large number of targets in a cell, with uniform distribution of position, speed and heading, then applying the target motion model to produce the destination cell of the target. For example, the diffusion matrix over a 1 minute interval for targets with uniformly distributed speed between 5 and 15 knots with a grid size of 1 km is

$$G = \begin{bmatrix} 0.0036 & 0.0582 & 0.0036 \\ 0.0582 & 0.7526 & 0.0582 \\ 0.0036 & 0.0582 & 0.0036 \end{bmatrix}. \quad (6)$$

The reduction in the threat map probabilities caused by a ping is calculated by applying a Bayesian update to each cell of the map; for an action $a \in \mathcal{A}$, the update is

$$P_{T,k}(a) = \frac{(1 - P_d(a)) P_{T,k-1}}{(1 - P_d(a)) P_{T,k-1} + (1 - P_{\text{fa}})(1 - P_{T,k-1})}, \quad (7)$$

where $P_{T,k}(a)$ is the updated probability that there is an undetected target in the cell once action a has been taken, $P_d(a)$ is the probability that a target in the cell is detected from action a and P_{fa} is the false alarm probability. Note that the probability $P_d(a)$ is obtained by generating many possible targets in each cell and averaging the probability of detection calculated by BRISE [17] over all targets.

Finally, the search reward for an action a is defined as

$$R_{\text{search}}(a) = \lambda \sum_x \sum_y P_{T,k}(x, y, a) - P_{T,k-1}(x, y) \quad (8)$$

This rewards transmissions that have high probability of detection in areas of the sonobuoy field that have not yet been searched for targets. Note that λ is a constant used to scale the search reward so it is comparable in magnitude to the tracking reward. This scaling is set to $\lambda = 6$ and equates to a rescaling of the value of α.

4. SIMULATION RESULTS

To analyse the performance of our scheduler, we vary α from 0 to 1 and perform 300 Monte-Carlo simulations, for each value of α, on the scenario illustrated in Fig. 1. This scenario comprises a 4×4 grid of transmitter sonobuoys, spaced 15 km apart, with a 5×5 grid of receiver sonobuoys, offset relative to the transmitters, and two targets to find and track. The scenario lasts for 50 minutes with a transmission every minute. The blue target is present for the whole duration and the green target appears after 10 minutes. The trajectories for these targets are generated using a noisy version of the constant velocity model defined in (1). The noise corruption is Gaussian in nature and drawn from $\mathcal{N}(\mathbf{0}, \mathbf{Q})$, where the variance $\mathbf{Q}$ is defined as

$$\mathbf{Q} = \omega \begin{bmatrix} T^3/2 & T^2/2 \\ T^2/2 & T \end{bmatrix} \otimes \mathbf{I}_2,$$

and ω is the intensity of the noise. Lastly, the depth of each target is fixed to 55m and the threat map $P_{T,0}$ is initialised with 0.0008 for all cells. This scenario is designed to test the ability of the scheduler to search for the green target while maintaining low track error for the known (blue) target.

We use two metrics to measure the performance of the proposed scheduler. The first measures the number of targets undetected by the scheduler. This number is computed by first assigning the confirmed tracks, given by the tracker, to the targets in a way that minimises the total distance between tracks and targets. Then any targets that are not assigned to tracks, or are assigned to tracks that are a distance greater than some constant away (200 meters in this paper), are

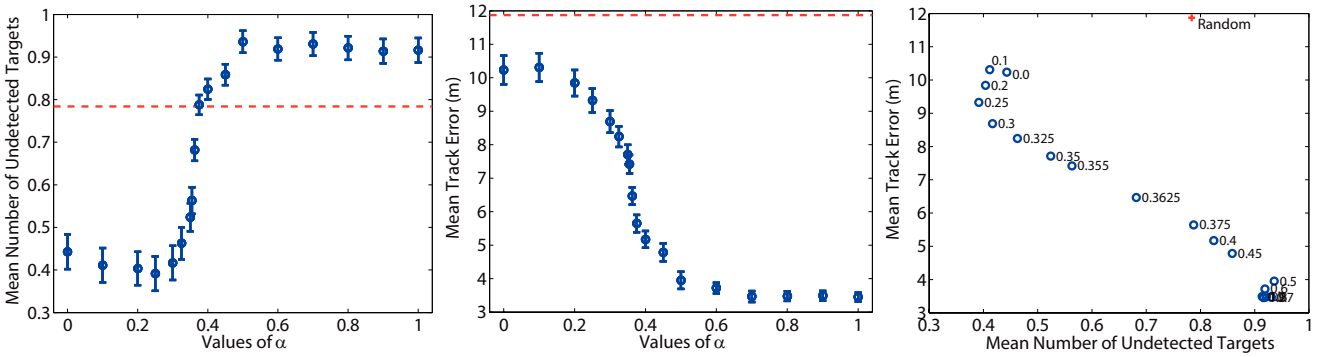

(a) Mean Undetected Targets (b) Mean Track Error (m) (c) Pareto-esque Frontier

Fig. 2. Performance of the Scheduler. Part (a) shows the mean number of undetected targets as the value of α varies from 0 to 1, part (b) shows the mean track error for the same values of α and part (c) combines both errors to give a Pareto-esque frontier for the scheduler. The red dashed line (and '+') indicates the performance obtained using random scheduling. The error bars indicate the 95% confidence intervals.

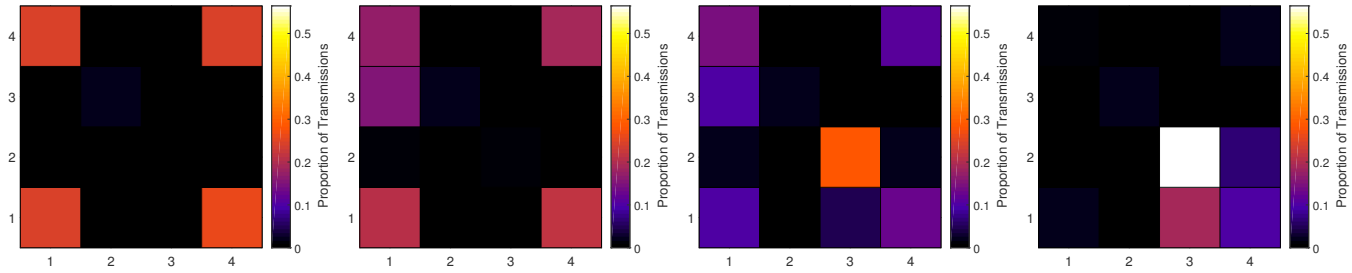

(a) $\alpha = 0.0$ (b) $\alpha = 0.25$ (c) $\alpha = 0.3625$ (d) $\alpha = 1.0$

Fig. 3. Transmitter histograms for the scenario illustrated in Fig. 1. The histograms show the proportion of waveforms transmitted from each source for four values of α over the 300 Monte Carlo runs. Note that each cell represents a transmitter in the field and the grid orientation corresponds to field geometry shown in Fig. 1.

counted as undetected targets. The mean number of undetected targets during a simulation is used to evaluate the search performance of the scheduler. The second metric evaluates the performance of known target tracks. Using the same track assignment as the search metric, the tracking error is the mean Euclidean distance between confirmed tracks and targets, provided that this distance is less than 200m.

The performance results for the scheduler are shown in Fig. 2. Part 2(a) shows the mean number of undetected targets for various α and Part 2(b) shows the mean track error for the same values of α. The error bars on each graph indicate the 95% confidence intervals. As a comparison, the red dashed lines correspond to the mean performance obtained when randomly scheduling the sonobuoy field. Note that the values shown in the graphs are averaged over both the whole scenario time and the number of Monte Carlo simulations. The two metrics are then put on a single scatter plot in Part 2(c) to create a Pareto-esque front that characterises the search-track trade-off of the scheduler. The performance of the random scheduler is represented as a red '+'.

As expected, Fig. 2 demonstrates clearly the trade-off between search and tracking controlled by α; increasing α puts more emphasis on the tracking objective whereas decreasing α focuses the scheduler on searching. Interestingly, the number of undetected targets increases slightly as α decreases from 0.2 to 0. This variability probably arises because the scheduler loses track of known targets if they are not detected for some time. In terms of Pareto optimality, Fig. 2(c) shows that not all of the obtained solutions are Pareto optimal. For example, using $\alpha = 0.25$ results in smaller tracking and search errors than all lower values of α. As a consequence, the Pareto front constitutes the points corresponding to $\alpha \in [0.25, 0.45]$ and $\alpha \in [0.6, 1.0]$. Fig. 2(c) also demonstrates that intelligent scheduling of the transmitters, regardless of the value of α, significantly outperforms random scheduling.

To further analyse the behaviour of the scheduler, histograms of the sources selected to transmit a waveform during the simulations are shown in Fig. 3. The figure shows how the scheduling of the sources changes as α increases from 0.0 to 1.0. Specifically, when $\alpha = 0.0$, in Fig. 3(a), the scheduler chooses sources around the perimeter to fulfill the search task. However, as α increases, the scheduler is more likely to choose sources that are closer to the targets. In particular, when $\alpha = 1.0$, in Fig. 3(d), the scheduler focuses on tracking the blue target thus choosing sources in the bottom right corner of the field.

5. CONCLUSION

We presented a multi-objective framework for scheduling in multistatic sonobuoy fields. Our framework is based on treating search and tracking tasks as competing objectives and using multi-objective optimization to decide the optimum source-waveform action at a given transmission time. These objectives were combined as a convex sum, where the weight parameter controls the priority the scheduler places on search and tracking. By varying the value of this weight, the trade-off between search and track in the scheduler can be characterized in terms of a set of points on the Pareto front. Using realistic multistatic sonobuoy simulations, we evaluated the performance of our scheduler and estimated the Pareto front for a particular scheduling scenario.

6. REFERENCES

[1] D. Krout, M. El-Sharkawi, W. Fox, and M. Hazen, "Intelligent ping sequencing for multistatic sonar systems," in *Proc. Int. Conf. Inf. Fusion (FUSION)*, Florence, Italy, 2006, pp. 1–6.

[2] D. Krout, W. Fox, and M. El-Sharkawi, "Probability of target presence for multistatic sonar ping sequencing," *IEEE J. Ocean. Eng.*, vol. 34, no. 4, pp. 603–609, 2009.

[3] B. I. Incze and S. Dasinger, "A Bayesian method for managing uncertainties relating to distributed multistatic sensor search," in *Proc. Int. Conf. Inf. Fusion (FUSION)*, Florence, Italy, 2006, pp. 1–7.

[4] S. Simakov and F. Fletcher, "GPU acceleration of threat map computation and application to selection of sonar field controls," in *Proc. Int. Conf. Acoust., Speech and Signal Process. (ICASSP)*, Brisbane, Australia, 2015, pp. 1827–1831.

[5] C. Y. Wakayama, D. J. Grimmett, and Z. B. Zabinsky, "Forecasting probability of target presence for ping control in multstatic sonar networks using detection and tracking models," in *Proc. Int. Conf. Inf. Fusion (FUSION)*, Chicago, IL, USA, 2011, pp. 1–8.

[6] C. Y. Wakayama and D. J. Grimmett, "Adaptive ping control for track-holding in multistatic active sonar networks," in *Proc. Int. Conf. Inf. Fusion (FUSION)*, Edinburgh, UK, 2010, pp. 1–8.

[7] S. Suvorova, M. Morelande, B. Moran, S. Simakov, and F. Fletcher, "Ping scheduling for multistatic sonar systems," in *Proc. Int. Conf. Inf. Fusion (FUSION)*, Salamanca, Spain, 2014, pp. 1–8.

[8] A. Saksena and I. J. Wang, "Dynamic ping optimization for surveillance in multistatic sonar buoy networks with energy constraints," in *IEEE Conf. Decision Control*, Cancun, Mexico, 2008, pp. 1109–1114.

[9] C. Y. Wakayama, Z. B. Zabinsky, and D. J. Grimmett, "Linear optimization models with integer solutions for ping control problems in multistatic active acoustic networks," in *Proc. Int. Conf. Inf. Fusion (FUSION)*, Singapore, 2012, pp. 2354–2361.

[10] D. Angley, S. Suvorova, B. Ristic, W. Moran, F. Fletcher, H. Gaetjens, and S. Simakov, "Sensor scheduling for target tracking in large multistatic sonobuoy fields," in *Proc. Int. Conf. Acoust., Speech and Signal Process. (ICASSP)*, New Orleans, LA, USA, 2017, pp. 3146–3150.

[11] D. Angley, R. Ristic, S. Suvorova, B. Moran, F. Fletcher, H. Gaetjens, and S. Simakov, "Non-myopic sensor scheduling for multistatic sonobuoy fields," *IET Radar, Sonar & Navig.*, vol. 11, no. 12, pp. 1770–1775, 2017.

[12] R. T. Marler and J. S. Arora, "Survey of multi-objective optimization methods for engineering," *Struct. Multidiscipl. Optim.*, vol. 26, no. 6, pp. 369–395, 2004.

[13] H. W. Kuhn and A. W. Tucker, "Nonlinear programming," in *Proc. Second Berkeley Symp. Mathematical Statistics and Probability*. 1951, pp. 481–492, University of California Press, Berkeley.

[14] V. Pareto, "Manuale di economica politica, societa editrice libraria," *Manual of political economy*, vol. 1971, 1906.

[15] S. Sen, G. Tang, and A. Nehorai, "Multiobjective optimization of OFDM radar waveform for target detection," *IEEE Trans. Signal Process.*, vol. 59, no. 2, pp. 639–652, 2011.

[16] N. Cao, S. Choi, E. Masazade, and P. K. Varshney, "Sensor selection for target tracking in wireless sensor networks with uncertainty," *IEEE Trans. Signal Process.*, vol. 64, no. 20, pp. 5191–5204, 2016.

[17] S. Simakov, "Signal excess data and tools for multistatic sonar emulation," Tech. Report DSTO-TR-3026, DSTO, 2014.

[18] H. Weinberg and R. E. Keenan, "Gaussian ray bundles for modeling high-frequency propagation loss under shallow-water conditions," *J. Acoust. Soc. America*, vol. 100, no. 3, pp. 1421–1431, 1996.

[19] B. Ristic, D. Angley, F. Fletcher, S. Simakov, H. Gaetjens, S. Suvorova, and B. Moran, "Bayesian multitarget tracker for multistatic sonobuoy systems," in *Proc. Int. Conf. Inf. Fusion (FUSION)*, Heidelberg, Germany, 2016, pp. 2171–2178.

[20] F. Fletcher and S. Arulampalam, "A comparison of existence-based multitarget trackers for multistatic sonar," in *Proc. Int. Conf. Inf. Fusion (FUSION)*, Singapore, 2012, pp. 2362–2369.

[21] J. Georgy, A. Noureldin, and G. R. Mellema, "Clustered mixture particle filter for underwater multitarget tracking in multistatic active sonobuoy systems," *IEEE Trans. Syst. Man Cybern. C, Appl. Rev.*, vol. 42, no. 4, pp. 547–560, 2012.

[22] B.-T. Vo, C.-M. See, N. Ma, and W. T. Ng, "Multi-sensor joint detection and tracking with the Bernoulli filter," *IEEE Trans. Aerosp. Electron. Syst.*, vol. 48, no. 2, pp. 1385–1402, 2012.

[23] B. Ristic and A. Farina, "Target tracking via multi-static doppler shifts," *IET Radar, Sonar & Navig.*, vol. 7, no. 5, pp. 508–516, 2013.

[24] B. Ristic, B. T. Vo, B. N. Vo, and A. Farina, "A tutorial on Bernoulli filters: Theory, implementation and applications," *IEEE Trans. Signal Process.*, vol. 61, no. 13, pp. 3406–3430, 2013.

[25] D. Mušicki and B. La Scala, "Multi-target tracking in clutter without measurement assignment," *IEEE Trans. Aerosp. Electron. Syst.*, vol. 44, no. 3, pp. 877–896, 2008.

[26] B. Ristic, D. Angley, S. Suvorova, B. Moran, F. Fletcher, H. Gaetjens, and S. Simakov, "Gaussian mixture multitarget multisensor Bernoulli tracker for multistatic sonobuoy fields," *IET Radar, Sonar & Navig.*, vol. 11, no. 12, pp. 1790–1797, 2017.

[27] I. Das and J. Dennis, "A closer look at drawbacks of minimizing weighted sums of objectives for Pareto set generation in multicriteria optimization problems," *Struct. optimi.*, vol. 14, no. 1, pp. 63–69, 1997.

[28] D. J. Kershaw and R. J. Evans, "Optimal waveform selection for tracking systems," *IEEE Trans. Inf. Theory*, vol. 40, no. 5, pp. 1536–1550, 1994.

[29] M. L. Hernandez, T. Kirubarajan, and Y. Bar-Shalom, "Multisensor resource deployment using posterior Cramér-Rao bounds," *IEEE Trans. Aerosp. Electron. Syst.*, vol. 40, no. 2, pp. 399–416, 2004.

[30] C. Yang, L. Kaplan, and E. Blasch, "Performance measures of covariance and information matrices in resource management for target state estimation," *IEEE Trans. Aerosp. Electron. Syst.*, vol. 48, no. 3, pp. 2594–2613, 2012.

[31] B. Ristic, S. Arulampalam, and N. Gordon, "Beyond the Kalman filter: Particle filters for tracking applications," *Artech House*, 2004.